Ultrasound in Med. & Biol., Vol. 40, No. 1, pp. 210–221, 2014

0301-5629/$ - see front matter

http://dx.doi.org/10.1016/j.ultrasmedbio.2013.09.013

● *Original Contribution*

DOPPLER VORTOGRAPHY: A COLOR DOPPLER APPROACH TO QUANTIFICATION OF INTRAVENTRICULAR BLOOD FLOW VORTICES

Forough Mehregan,*† François Tournoux,‡ Stéphan Muth,*† Philippe Pibarot,§ Régis Rieu,‖ Guy Cloutier,†¶# and Damien Garcia*†#

*RUBIC, Research Unit of Biomechanics & Imaging in Cardiology, University of Montreal Hospital, Montreal, QC, Canada; †CRCHUM, Research Center, University of Montreal Hospital, Montreal, QC, Canada; ‡Department of Echocardiography, CHUM, University of Montreal Hospital, Montreal, QC, Canada; §Department of Medicine, Laval University and Québec Heart & Lung Institute, Laval University, Montreal, QC, Canada; ‖Aix-Marseille University, CNRS, UMR 7287, ISM, GIBOC, Marseille, France; ¶LBUM, Laboratory of Biorheology and Medical Ultrasonics, University of Montreal Hospital, Montreal, QC, Canada; and #Department of Radiology, Radio-Oncology and Nuclear Medicine and Institute of Biomedical Engineering, University of Montreal, Montreal, QC, Canada

(*Received* 18 *June* 2013; *revised* 5 *September* 2013; *in final form* 9 *September* 2013)

Abstract—We propose a new approach to quantification of intracardiac vorticity based on conventional color Doppler images —Doppler vortography. Doppler vortography relies on the centrosymmetric properties of the vortices. Such properties induce particular symmetries in the Doppler flow data that can be exploited to describe the vortices quantitatively. For this purpose, a kernel filter was developed to derive a parameter, the blood vortex signature (BVS), that allows detection of the main intracardiac vortices and estimation of their core vorticities. The reliability of Doppler vortography was assessed in mock Doppler fields issued from simulations and *in vitro* data. Doppler vortography was also tested in patients and compared with vector flow mapping by echocardiography. Strong correlations were obtained between Doppler vortography-derived and ground-truth vorticities (*in silico*: $r^2 = 0.98$, *in vitro*: $r^2 = 0.86$, *in vivo*: $r^2 = 0.89$). Our results indicate that Doppler vortography is a potentially promising echocardiographic tool for quantification of vortex flow in the left ventricle. (E-mail: damien.garcia@crchum.qc.ca or garcia.damien@gmail.com) © **2014 World Federation for Ultrasound in Medicine & Biology.**

Key Words: **Doppler echocardiography, Intraventricular blood flow, Vortex imaging, Vorticity, Doppler vortography, Vector flow mapping.**

INTRODUCTION

Within the left ventricle of a normal heart, diastolic filling is characterized by the formation of a swirling motion during early filling (Gharib et al. 2006; Kilner et al. 2000; Toger et al. 2012): A large diastolic vortex forms adjacent to the anterior mitral valve leaflet and rotates in the natural flow direction. In the normal heart, a large part of the left ventricular (LV) blood volume is actually involved in the vortex formation. Because flowing blood keeps moving at the end of diastole, flow transition to ejection is ensured, which makes systole tightly coupled with diastolic filling (Carlhall and Bolger 2010; Chan and Veinot 2011). Accordingly, recent *in vitro* and *in vivo* observations suggest that the normal vortex pattern might minimize the fluid energy dissipation and optimize LV myocardial efficiency (Charonko et al. 2013; Domenichini et al. 2007; Kilner et al. 2000; Pedrizzetti and Domenichini 2005). Vortices that form during LV filling thus have specific geometries and locations, which could be determinant factors of heart function (Hong et al. 2008; Nucifora et al. 2010). In patients with abnormal heart filling, there is an impairment of the wall/fluid dynamics that may disturb the flow patterns and, thus, affect the diastolic vortical structures (Nucifora et al. 2010). Reliable tools for imaging the intraventricular flow arrangements could be of major clinical interest for a better assessment of LV diastolic function. Comprehensive intracardiac velocity mapping can be measured by phase-contrast magnetic resonance imaging (MRI).

Address correspondence to: Damien Garcia, CRCHUM, Pavillon JA de Sève Local Y-1619, 2099 Alexandre de Sève, Montreal, QC H2L 2W5, Canada. E-mail: damien.garcia@crchum.qc.ca or garcia.damien@gmail.com

Acquisition of 3-D cine phase contrast velocity data can indeed provide time-resolved characterization of blood flow in the left ventricle (Eriksson et al. 2010; Markl et al. 2011; Mohiaddin 1995; Toger et al. 2012; Wigstrom et al. 1999). MRI, however, is difficult to implement in routine practice because of limited accessibility and cost. Besides MRI, several echocardiographic techniques have been proposed in the last two decades to make vortex imaging more easily available for clinical daily practice. So far, four principal echocardiographic techniques have been described:

1. The earliest echographic studies regarding diastolic flow patterns are those based on observations from 2-D color Doppler and color M-mode echocardiography (Delemarre et al. 1990; Rodevand et al. 1999; Van Dantzig et al. 1995). Normal and abnormal flows were defined qualitatively according to the diastolic arrangements of the Doppler spectrum waveforms or of the red/blue-encoded Doppler velocities in the left ventricle. No quantitative measures of the vortices, however, were proposed.
2. Vortex formation time (VFT) has recently been proposed as an echocardiographic parameter to quantify the formation of LV vortices. VFT is a nondimensional index that characterizes the optimal conditions leading to vortex formation (Dabiri and Gharib 2005). It has also been claimed to be an index of cardiac function (Gharib et al. 2006). Recent clinical studies in acute cardiomyopathy have reported that VFT is reduced with impaired relaxation (Jiamsripong et al. 2009; Kheradvar et al. 2012; Nucifora et al. 2010; Poh et al. 2012). The VFT index, however, is simply a surrogate parameter that is calculated from standard echographic measures (stroke volume, mitral valve diameter, E and A waves). As a consequence, similarly to these standard parameters, it is expected that the VFT index may lack consistency in some situations. Whether this index is of clinical interest still remains questionable (Stewart et al. 2012).
3. Echo-particle image velocimetry (echo-PIV) is an efficient echographic tool for intraventricular velocity mapping (Cimino et al. 2012; Hong et al. 2008; Prinz et al. 2012). This technique, applied to contrast-enhanced echocardiographic images, is able to track ultrasound speckle displacements to estimate blood motion within the image plane (Gao et al. 2012; Kim et al. 2004). Recent studies have focused on LV vortex quantification by echo-PIV (Cimino et al. 2012; Faludi et al. 2010; Hong et al. 2008; Sengupta et al. 2012). This technique requires a continuous intravenous injection of contrast agent to reach an image quality suitable for motion tracking (Gao et al. 2012), seriously limiting the application of echo-PIV in daily clinical practice.
4. Cardiac Doppler vector flow mapping (VFM) is a technique based on 2-D color Doppler images and, thus, can be easily used for clinical applications. In the VFM approach, 2-D assumptions are used to develop an intracardiac vector distribution by deducing the velocity components perpendicular to the ultrasound beam within the entire Doppler field. Several techniques for intraventricular VFM have been recently been proposed (Arigovindan et al. 2007; Garcia et al. 2010; Uejima et al. 2010). Preliminary studies indicated promising results regarding the feasibility of LV vortex quantification in patients by VFM (Chen et al. 2012; Hendabadi et al. 2013; Lu et al. 2012; Zhang et al. 2012). Additional studies are still required to determine the accuracy and clinical reproducibility of Doppler VFM.

The new technique we propose—Doppler vortography—has been developed specifically to detect and quantify the intraventricular vortices that form during LV filling. Doppler vortography targets mainly particular local flow patterns present in the Doppler field using a fast detection algorithm. To detect and quantify the vortices, we propose an index called the "blood vortex signature" (BVS), obtained using a specific covariance-based kernel filter. This approach is thoroughly described in the next section. It is shown that Doppler vortography can estimate core vorticities accurately and that the results are concordant with those obtained by the vector flow mapping method.

METHODS

We here derive a new echocardiographic methodology, Doppler vortography, for detecting and quantifying the large-scale vortices that form in the left ventricle during diastolic filling. Figure 1 is a schematic example of vortex detection and quantification by Doppler vortography. As seen in this figure, for the particular case of a single large vortex, color Doppler exhibits an obvious antisymmetric imprint: negative mirror symmetry occurs with respect to the scan line crossing the vortex center. This anti-symmetry can also be used to detect intraventricular vortices. The Doppler vortography modality for intraventricular vortex imaging and the resulting BVS are described further below. *In silico* and *in vitro* studies were performed to validate the proposed technique and analyze the effects of transducer position and BVS filter kernel size. Doppler vortography was finally compared with VFM in patients using the VFM technique described by Garcia et al. (2010).

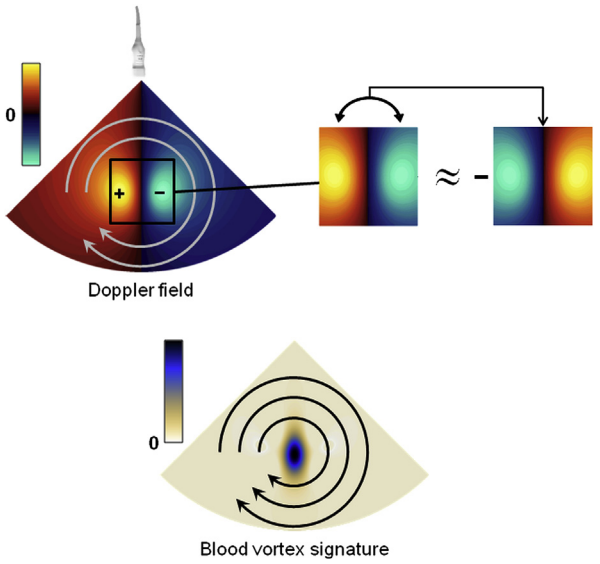

Fig. 1. Basic concept of Doppler vortography. For a single large vortex, color Doppler exhibits negative mirror symmetry with respect to the scan line crossing the vortex center (*top*). The proposed parameter, "blood vortex signature," allows detection of the vortex center from this antisymmetric property (*bottom*) (see also Fig. 2).

Assuming that the vortices are nearly axisymmetric around their center, the vorticity, which describes the local rotational characteristics of the fluid, is estimated at the core of the detected vortices. In the following, because we focus on ultrasound cardiac imaging, the Doppler data are represented in a polar coordinate system (r, θ) whose origin is related to the location of the phased-array transducer. In this configuration, the Doppler velocities are thus given by the radial components of the velocity field.

Theoretical concept of Doppler vortography

A vortex is a particular flow arrangement that has a rapid swirling motion around its center. It is characterized mainly by its core vorticity, which somewhat reflects the "strength" of the spinning flow. As an ultrasound probe scans across a vortical flow whose scale is significantly larger than the ultrasound beam width, the Doppler field is characterized by a specific configuration that can be exploited to describe the vortex quantitatively: because of the centrosymmetric nature of a vortex, scanning such a flow pattern yields mainly a scan line of zeroes surrounded by two maxima of opposite signs (Fig. 1). Doppler vortography simply relies on this antisymmetric property. Because of the nearly rotational symmetry of a vortex, it is also noted that flipping left to right a small kernel centered on the vortical core mostly modifies its sign only (Fig. 1). Mathematically speaking, if (r_c, θ_c) denotes the polar coordinates of the vortex center, the Doppler velocities V_D about (r_c, θ_c) nearly follow an odd function with respect to the angular component:

$$V_D(r, \theta-\theta_c) \approx -V_D(r, -(\theta-\theta_c)) \quad \text{if} \quad r \approx r_c \text{ and } \theta \approx \theta_c. \tag{1}$$

To detect the locations (r_c, θ_c) of the vortex cores, one can seek the regions where the Doppler velocity follows eqn (1). For this purpose, we developed a simple kernel filter that returns a parameter (BVS) that reaches an extremum at a vortex core. We recall that we work on a regular polar grid $(r_i, \theta_j)_{i\,=\,1\ldots M,\ j\,=\,1\ldots N}$, where $M \times N$ is the size of the raw Doppler field (Fig. 2). Let $\mathbf{w}_D^{ij}$ represent a block of size $(2m + 1) \times (2n + 1)$ centered on (r_i, θ_j) and given by

$$\mathbf{w}_D^{ij} = [V_D(r_k, \theta_l)]_{k\,=\,i-m\ldots i+m, l\,=\,j-n\ldots j+n}. \tag{2}$$

The BVS parameter is now defined as (Fig. 2)

$$\mathrm{BVS}_{ij} = \mathrm{BVS}(r_i, \theta_j) = R(\mathrm{cov}(\mathbf{w}_D^{ij}, -\mathrm{fliplr}(\mathbf{w}_D^{ij}))) \times S_{ij} \tag{3}$$

where R and cov stand for the ramp and covariance functions, respectively. The operator "fliplr" flips the matrix $\mathbf{w}_D^{ij}$ left to right, that is, in the angular direction. According to eqn (1), $\mathbf{w}_D^{ij} \approx -\mathrm{fliplr}(\mathbf{w}_D^{ij})$ if the window $\mathbf{w}_D^{ij}$ is centered on a vortex core; the covariance operator allows one to detect where this equality occurs. The ramp function R is used in eqn (3) because the negative covariance values are of no interest in this study. The rightmost term S_{ij} in eqn (3) is a scalar (=1 or –1), which reflects the direction of the vortex (clockwise: 1, counterclockwise: –1). It is determined by using

$$S_{ij} = \mathrm{sgn}\left(\sum_{k,l} (\mathbf{w}_D^{ij}(k, l-1) - \mathbf{w}_D^{ij}(k, l)) \right) \tag{4}$$

where sgn is the signum function. Because of the covariance measure in eqn (3), the BVS yielded by Doppler vortography has high amplitude at the vicinity of a vortex and reaches a local extremum at its center (see an example in Fig. 3 based on a vortex pair). As such, the BVS parameter can help to detect the vortical structures that form in the left ventricle during early filling. It could also be of clinical interest to quantify them. A vortex is described mainly by its core vorticity. The vorticity ω in polar coordinates (r, θ) is given by the curl of the vector field

$$\omega = \frac{1}{r}\left(\frac{\partial}{\partial r}(r\ V_\theta) - \frac{\partial V_r}{\partial \theta} \right), \tag{5}$$

where V_r and V_θ are the radial and angular velocity components, respectively. The Doppler velocities (V_D) are related to the radial velocities as follows: $V_r = -V_D$.

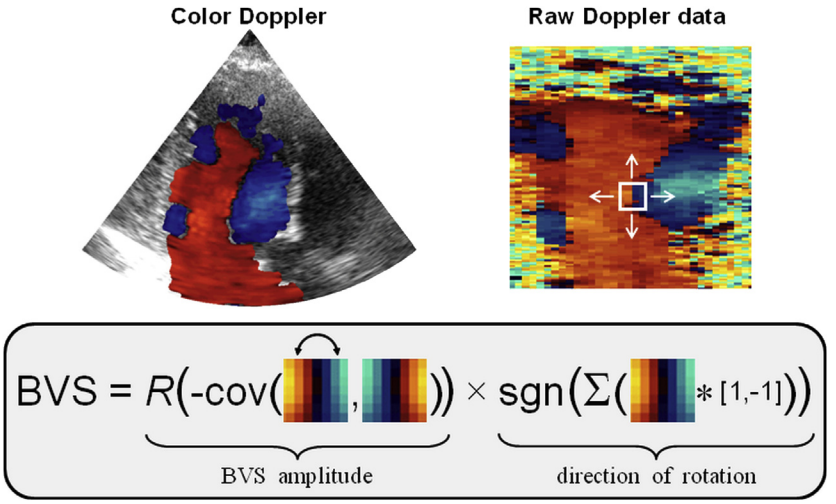

Fig. 2. Blood vortex signature. The blood vortex signature (BVS) is calculated using a small block sliding over the raw color Doppler array. The local BVS is based on the covariance (cov) between this block and its antisymmetric counterpart. The rotation direction is determined using a simple convolution. *R* and sgn stand for the ramp and sign functions, respectively.

Assuming now that the vortex is axisymmetric at the vicinity of its core, one has, at the center of the vortex located at (r_c, θ_c),

$$\frac{\partial}{\partial r}(r\ V_\theta) = \frac{-\partial V_r}{\partial \theta}, \quad \text{if} \quad (r,\theta) = (r_c,\theta_c) \tag{6}$$

By use of eqns (5) and (6), the core vorticity ω_C can finally be written as a function of the Doppler velocities:

$$\omega_c = \left(\frac{-2}{r}\frac{\partial V_r}{\partial \theta}\right)\Bigg|_{r_c,\theta_c} = \frac{2}{r_c}\frac{\partial V_D}{\partial \theta}\Bigg|_{r_c,\theta_c}. \tag{7}$$

To sum up, Doppler vortography works as follows: (i) The BVS is measured during diastole from the color Doppler data using eqn (3). (ii) The main vortices are detected by seeking the extrema of BVS. (iii) Their core vorticities are estimated using eqn (7).

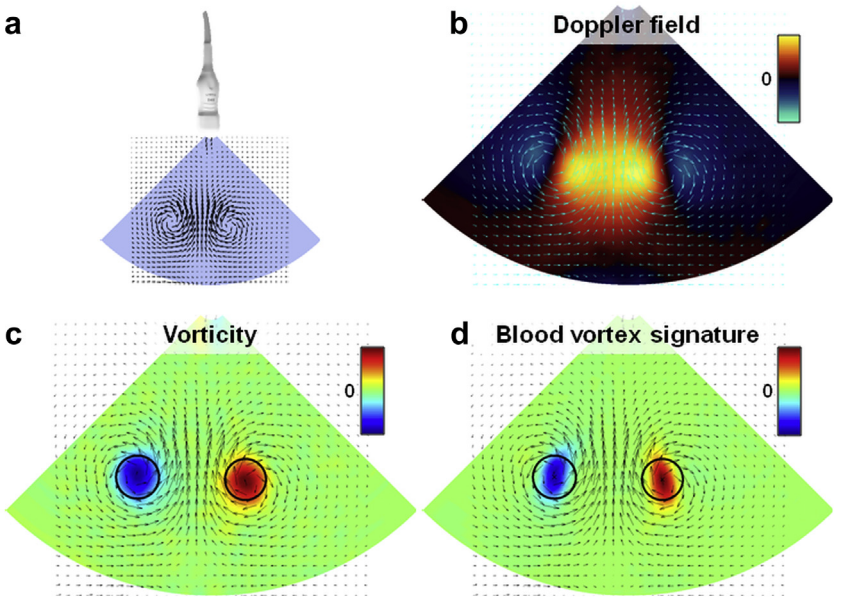

Fig. 3. Doppler vortography for a vortex pair. Insonification of a vortex pair (a) and corresponding mock color Doppler field (b). The "blood vortex signature" (BVS) parameter reaches an extremum at the vortex core (d). As a comparison, the ground-truth vorticity field is also depicted (c).

Numerical simulations

To test the accuracy of Doppler vortography under ideal conditions, numerical ultrasound simulations were first performed with a Lamb-Oseen vortex. The Lamb-Oseen vortex is a commonly used vortex model in fluid dynamics. The circumferential velocity component V_Φ of this vortex is given by

$$V_\Phi(\rho) = V_{\Phi_{\text{peak}}}\left(1+\frac{0.5}{\alpha}\right)\frac{\rho_c}{\rho}\left(1-e^{-\alpha\frac{\rho^2}{\rho_c^2}}\right) \quad (8)$$

where ρ is the distance from the vortex center, $\alpha \approx 1.2564$, $V_{\Phi_{\text{peak}}}$ is the peak circumferential velocity and ρ_c is the core radius. From eqn (5), the core vorticity (at $\rho = 0$) for a Lamb-Oseen vortex is deduced as

$$\omega_c = \frac{2\alpha+1}{\rho_c} V_{\Phi_{\text{peak}}} \quad (9)$$

The ultrasound simulations were performed using the freeware Field II developed by Jensen and Svendsen (Jensen 1996; Jensen and Svendsen 1992). A 64-element phased-array probe with a 0.3-mm pitch was simulated. A total of 40,000 randomly positioned coplanar scatterers—ensuring fully developed speckles—were insonified at 2.5 MHz with pulses containing eight cycles. The region of interest was 4 cm wide and ranged from 4 to 8 cm in depth respective to the probe. The Lamb-Oseen vortices were all centered within this region of interest. For a given vortex configuration, radiofrequency (RF) images containing 64 scan lines and covering a 40° wide sector were created at a pulse repetition frequency of 7 kHz. The consecutive RF images were generated after the scatterers had been displaced according to the Lamb-Oseen velocity field. The Doppler signals were calculated from the demodulated RF images using a standard auto-correlator (Kasai et al. 1985) with a packet size of 5. A total of 31 vortex configurations were simulated. To generate these scenarios, the vortex core radius (ρ_c) was fixed at 1, 1.25 and 1.5 cm, and the peak velocity ($V_{\Phi_{\text{peak}}}$) ranged from 0.35 to 1.5 m/s. These values were chosen to be consistent with clinical observations (Garcia et al. 2010). The Doppler fields were de-aliased and smoothed using an unsupervised denoising method (Garcia 2010; Muth et al. 2011). For each Doppler field, the BVS was calculated from the simulated polar Doppler data using eqn (3), and the vortex core was located from the BVS extremum (Fig. 4). Several kernel sizes, that is, $(2n + 1) \times (2n + 1)$, where $n = 1 \ldots 5$, were tested to analyze the robustness of the method. The effect of kernel size was analyzed using a repeated-measures analysis of variance (MedCalc Software, Version 12.5, Ostend, Belgium). The core vorticity was finally estimated using eqn (7) and compared with the ground-truth vorticity (eqn [9]) using a linear regression and a Bland-Altman plot.

In vitro data

The Doppler fields simulated with Field II were all based on perfectly axisymmetric vortices. Additional simulations were also performed with more realistic vortical patterns issued from *in vitro* data. These *in vitro* experiments were performed using an atrio-ventricular dual-activation pulse duplicator (courtesy of ESIL, Marseilles, France). As previously described in Garcia et al. (2010), this *in vitro* model consists of ventricular and atrial activation boxes, systemic and pulmonary circulation models and a computerized driving interface (Tanné et al. 2010). The left heart cavities are compliant and transparent. A liquid made of 40% glycerol and 60% saline water was used as a blood substitute. The *in vitro* system was set to simulate three different hemodynamic conditions: heart rate (bpm)/stroke volume (mL) = 60/65, 80/60 and 100/75. The velocity field within the ventricular cavity was measured using optical laser-based PIV. The laser plane cut the mitral and aortic valve planes, as well as the apex, to simulate an apical three-chamber view. The image series was processed with a standard commercial software

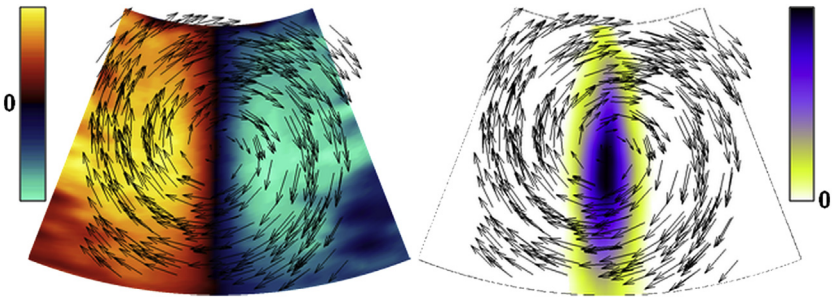

Fig. 4. In silico studies. Color Doppler fields were simulated in Lamb-Oseen vortices using Field II (*left*). The blood vortex signature was deduced from the color Doppler data using eqn (4) and allowed detection of the vortex core (*right*). The core vorticity yielded by Doppler vortography (eqn [7]) was compared with the theoretical core vorticity (eqn [9]) (see also Fig. 6).

package (Insight3 G, TSI, Shoreview, MN, USA). Ensemble average velocity fields were obtained using 30 consecutive heart cycles. The PIV data were post-processed by means of an unsupervised regularizer (Garcia 2011), and the vorticity was estimated using the eight-point method (Raffel et al. 2007). Through use of these PIV fields, 200 × 64 mock Doppler fields were simulated using Field II with the transducer located at the apical position. The parameters governing the simulations were similar to those reported in the previous subsection. The BVS was calculated using eqn (3) with different kernel sizes (an example is given in Fig. 5). The local extremum of the BVS patch corresponding to the main diastolic vortex (see Fig. 5) was detected, and the core vorticity was estimated using eqn (7). Doppler vortography-derived core vorticities (Eq. 7) were compared with those measured from the original PIV field (eight-point method) using standard linear regression and a Bland-Altman plot. They were both measured at the same location, that is, where the BVS amplitude was found to be maximal. This analysis was performed on the frames related to diastolic filling only (total = 14 frames). To determine if transducer position affects the results returned by Doppler vortography, several probe angles relative to the left ventricle centroid were tested (0°, ±5°, ±10°) (see Fig. 5). The effects of kernel size and probe angle were analyzed independently using repeated-measures analyses of variance (MedCalc Software, Version 12.5, Ostend, Belgium).

Clinical data

The core vorticities obtained with the new Doppler vortography method were compared with those obtained by the vector flow mapping technique developed by Garcia et al. (2010). In the latter method, the cross-beam velocity components are deduced from the 2-D continuity equation with adequate boundary conditions (see Garcia et al. [2010] for details). Doppler echocardiographic images were acquired using a Vivid 7 ultrasound system (GE Healthcare, USA) in 19 patients (5 men, 14 women, mean age = 57 ± 16 y). The use of these echographic images was approved by our local ethics committee. Informed consent was received from each participant. Among these patients, 12 were normotensive and 7 were hypertensive. They all had transthoracic echo considered as normal using common parameters. Apical three-chamber views with color Doppler over the entire left ventricular cavity were acquired during one to three cardiac cycles. The raw color Doppler data were exported from commercially available software (EchoPAC System, General Electric). A total of 55 frames were selected (average of 2.9 frames/patient). Only the frames obtained during early filling were considered in this study. Color Doppler data were analyzed using both Doppler vortography (eqns [3], [4] and [7]) and the vector flow mapping method proposed by Garcia et al. (2010). The core vorticity of the main mitral vortex (*i.e.*, the vortex at the tip of the anterior mitral valve leaflet) was estimated by Doppler

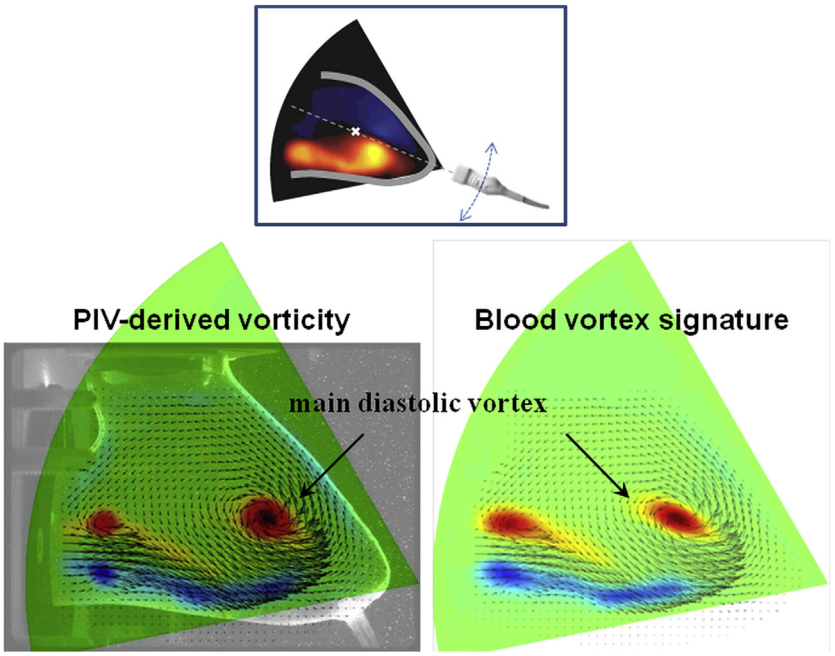

Fig. 5. In vitro data. Color Doppler fields were created from *in vitro* intraventricular particle image velocimetry (PIV) velocity fields. The blood vortex signature was measured by Doppler vortography, and the vorticity of the main diastolic vortex was compared with the PIV-derived vorticity. Several insonification angles were tested (see also Fig. 7).

vortography as described under Theoretical Concept of Doppler Vortography. As a reference, the core vorticity of the same vortex was also calculated using the vector flow technique as previously developed by Garcia et al. (2010): the Okubo-Weiss criterion for vortex detection was derived from the vector velocity fields, and the corresponding core vorticities were determined. The Okubo-Weiss criterion, also known as the Q criterion, is related to the second invariant of the velocity gradient tensor. Positive values point out the regions where vorticity prevails over strain rate (Hunt et al. 1988). Doppler vortography-derived core vorticities (eqn [7]) were compared with those measured by VFM using a standard linear regression and a Bland-Altman plot.

RESULTS

In silico and in vitro data: vortography-derived versus ground-truth vorticity

We observed good concordance between the vorticities estimated by Doppler vortography and those derived by control methods (*in silico*: analytical solution, *in vitro*: eight-point method). A strong correlation was obtained both *in silico* and *in vitro* ($r^2 = 0.98$ and $r^2 = 0.86$) (see Figs. 6 and 7), with reasonably small relative errors *in silico* (Fig. 6, right). As revealed by the Bland-Altman plot (Fig. 7, right), however, overestimations and higher relative errors were observed *in vitro* ($21 \pm 15\%$). This was due to the geometry of the vortices, whose cores were somewhat elliptic in the *in vitro* setup.

In silico and in vitro data: effects of kernel size and angle insonification

The repeated-measures analyses of variance revealed a significant effect of kernel size ($p < 0.001$), both *in silico* and *in vitro*. There was a negative linear trend ($p < 0.0001$) between kernel size and vorticity: that is, vorticity decreased with increasing kernel size. Pairwise comparisons, however, indicated that the mean vorticity differences between the 3×3 and 11×11 kernel configurations were $9.2 \pm 0.8\ s^{-1}$ (*in silico*) and $12.3 \pm 2.1\ s^{-1}$ (*in vitro*); these differences remained relatively small compared with the actual vorticity values (mean $> 190\ s^{-1}$). No significant effect of insonification angle ($p > 0.05$) was reported for the *in vitro* data. It can be concluded that kernel size and insonification angle had a negligible or no effect on the vorticity estimation.

In vivo study: Doppler vortography versus VFM-derived vorticity

Very good concordance between the vorticities estimated by Doppler vortography and VFM ($y = 2.2 + 0.95x$, $r^2 = 0.89$, $N = 55$, $p < 0.001$) was observed in 19 patients (Fig. 8, left). The relative error between the two methods was $2.7 \pm 14\%$ (Bland-Altman plot in Fig. 8). These findings indicate that good estimates of core vorticities can be obtained without the full vector components. To visually compare Doppler vortography and VFM, three examples are provided in Figure 9. The BVS maps returned by Doppler vortography (Fig. 9, second column) correlated well with the Okubo-Weiss criterion (Fig. 9, third column). Although these parameters are not aimed at being similar, they both allow vortex detection.

DISCUSSION

We have found that the echocardiographic tool that we derived, designated as Doppler vortography, can accurately detect and quantify the main intraventricular vortices that form during diastole. Intracardiac flow organization can be a robust marker of left ventricular filling. Blood flow is indeed very sensitive to its environment: as a fluid, and in contrast to solids, blood (on the macro scale) does not have a preferred shape because it does not possess any elastic behavior. In other words, a solid resists distortion, but fluid does not: contrary to solids, when a shear stress is applied to a fluid, the fluid continuously deforms. As a consequence, small dynamic and/or geometric perturbations may induce significant changes

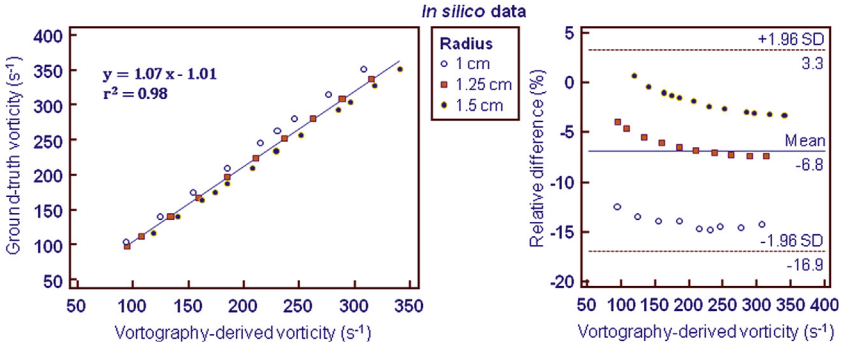

Fig. 6. In silico results. Comparison between vortography-derived (eqn [7]) and ground-truth (eqn [9]) vorticities. Different vortex core radii were simulated (see eqn [8]). SD = standard deviation.

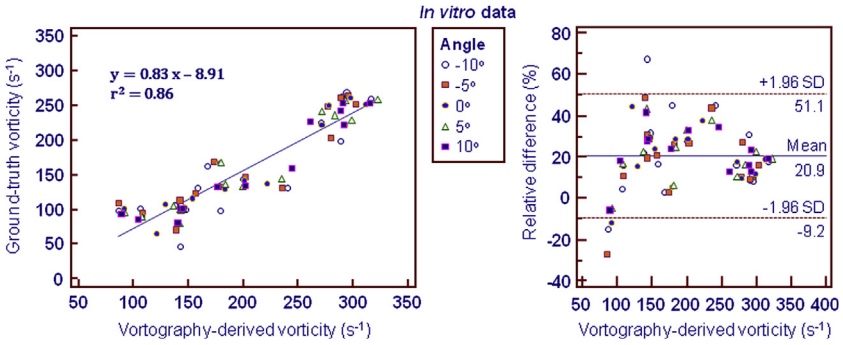

Fig. 7. In vitro results. Comparison between vortography-derived (eqn [7]) and ground-truth (eqn [9]) vorticities. Several angle insonifications were simulated (see Fig. 5). SD = standard deviation.

in flow patterns. For instance, in vascular flow, a slight modification in vessel geometry or flow dynamics, such as a bend, sharpness or acceleration, may modify blood flow patterns drastically. This phenomenon may be also true in the left ventricle and could be visible in the vortical structures (Kheradvar and Pedrizzetti 2012). It is thus anticipated that vortex analysis may provide additional information on left ventricular function. Concordantly, recent scientific literature reveals an emerging clinical interest in the characterization of intraventricular flow vortices (Belohlavek 2012; Cimino et al. 2012; Kheradvar et al. 2012; Poh et al. 2012; Toger et al. 2012). In this context, it was the aim of this study to propose a new color Doppler technique, Doppler vortography, for intraventricular vortex flow imaging. Because this technique makes use of conventional Doppler fields, Doppler vortography is fast, is clinically compliant and does not modify the clinical echo-lab routine.

Why use the three-chamber view?

In this study, we focused on the large vortical structures occurring in the apical long-axis three-chamber view. This plane passes through the apex and the centers of the mitral and aortic valves. Although intracardiac flow is known to be 3-D, phase-contrast MR studies have indicated that the out-of-plane velocity components are small in the plane corresponding to the echo three-chamber view (Eriksson et al. 2010, 2012; Wigstrom et al. 1999). Indeed, velocity data obtained by Wigstrom et al. (1999) and Eriksson et al. (2010, 2012) from 4-D phase contrast MR distinctly depict an intraventricular flow that is mainly parallel to the long-axis plane. In addition, clinically useful parameters of intraventricular flow dynamics can be obtained from a planar flow simplification using this view. In particular, Thompson and McVeigh (2003) reported that accurate pressure differences can be calculated using 2-D acquisitions because the momentum fluxes normal to the plane of interest are negligible. From these independent studies, it can be claimed that the utilization of 2-D statements in the particular three-chamber view is quite acceptable for analysis of the main flow vortices in most situations. We thus assumed that the main flow arrangements remain measurable in the three-chamber view, without significant loss of information. This assertion, however, may be invalid in severely diseased patients, in whom the 3-D nature of the flow could adversely influence Doppler vortography. Indeed, in such cases, the "anti-symmetry" hypothesis (see Fig. 1) could become ineffective. Further

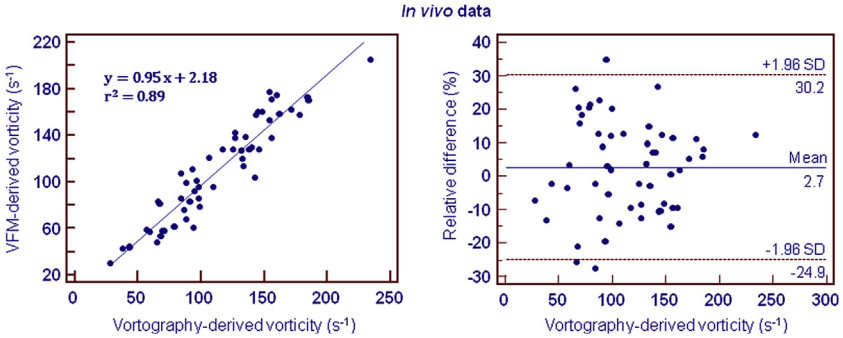

Fig. 8. In vivo results. Comparison between vortography-derived (eqn [7]) and vector flow mapping (VFM)-derived vorticities. Sample size = 55 color Doppler frames in 19 patients. See Figure 9 for three examples.

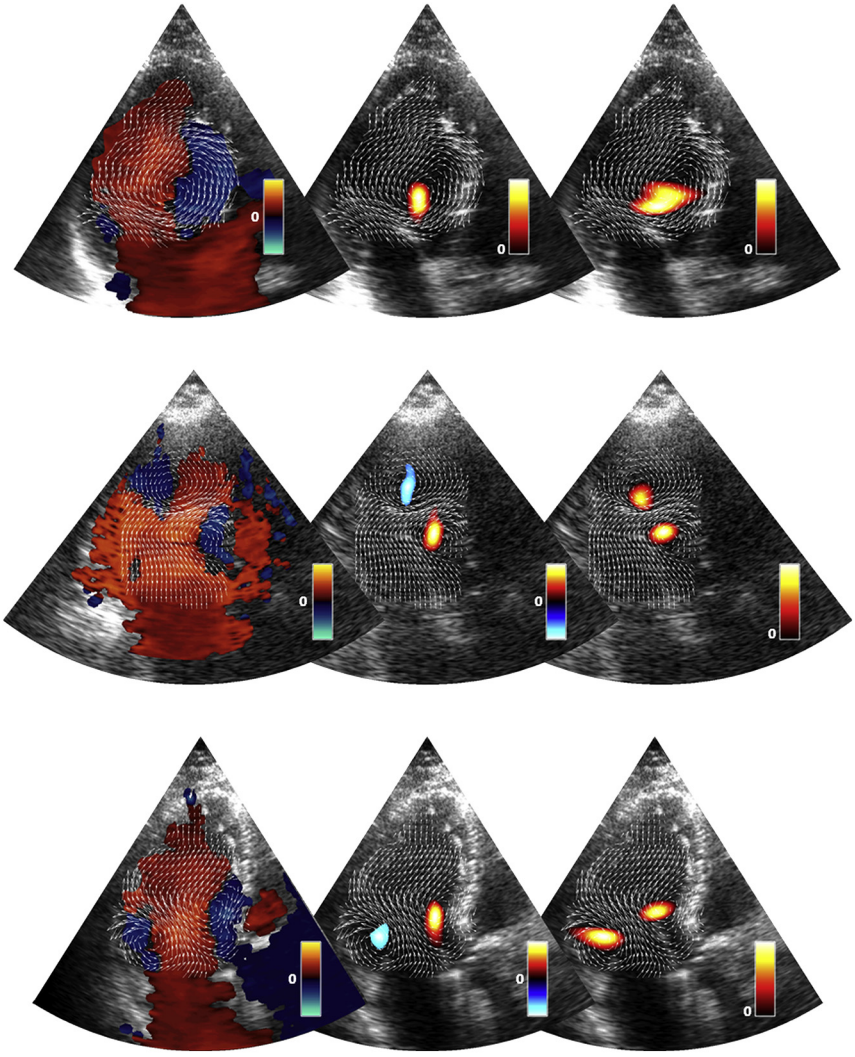

Fig. 9. Vector flow mapping (VFM) and Doppler vortography in three patients. The first column represents vector flows, as measured by the VFM technique described by Garcia et al. (2010), superimposed on conventional color Doppler images (the color bars represent Doppler velocities). In the second column are blood vortex signature (BVS) maps. High BVS amplitudes denote the presence of a large-scale vortex. The BVS sign represents the direction of rotation (see eqn [3]). The vector flows measured by VFM are also displayed for comparison purposes. The third column represents the Okubo-Weiss criterion derived from the VFM vector velocity fields. The Okubo-Weiss criterion is positive in zones of high vorticity. Note how well zones of high-amplitude BVS compare with this criterion. The images in the first row are from a normotensive subject with normal echo.

validation in mildly to severely diseased patients using velocimetry by cardiac magnetic resonance will help to better identify the physiologic conditions under which the 2-D hypothesis remains valid.

Doppler vortography versus vector flow mapping

Velocimetry by echo-PIV or phase-contrast MRI (see Introduction) would have been better gold standards than VFM, as these two techniques do not assume a planar flow. In contrast to the MRI and contrast echo approaches, however, Doppler vortography has the great advantage of being readily suitable for the clinical practice. Several techniques have been proposed for intracardiac vector flow mapping from conventional 2-D echocardiography, three of the most important ones being those described by Arigovindan et al. (2007), Garcia et al. (2010) and Uejima et al. (2010). The method proposed by Arigovindan et al. is not well adapted to cardiac flow imaging because two measurements differing by a significant angle are required. Although their theoretical concepts are different, the VFM approaches proposed by Uejima et al. and Garcia et al. are both based on single-color Doppler data set. The latter tactic minimizes the 2-D divergence to deduce the cross-beam velocity components

and has been found to be an accurate quantitative method (Garcia et al. 2010); this is the VFM technique that was used in patients in our study. VFM, as Doppler vortography, is based on color Doppler data only. However, it uses a different numerical approach; this VFM method thus does not necessarily yield axisymmetric vortices. As depicted in Figure 8, we obtained very good concordance between Doppler vortography and VFM when determining the core vorticities in patients. When superimposing the velocity vectors yielded by VFM on the BVS map, it appeared that Doppler vortography was able to detect the main vortices adequately (see Fig. 9). From our simulations and *in vivo* data, it can be concluded that Doppler vortography is an efficient non-invasive method for detection and quantification of intraventricular vortices. Doppler vortography has the advantage of being numerically simpler and faster than VFM. More importantly, it directly targets the vortical flow patterns present in the color Doppler field using an original detection algorithm.

Technical limitations of Doppler vortography

Doppler vortography is based on 2-D color Doppler imaging and, thus, can be affected by the inherent Doppler artifacts, including aliasing, low signal-to-noise ratio, low angular and temporal resolutions and clutter signals (Mitchell 1990). The default clutter filter, as provided by the clinical GE ultrasound scanner, was used during the acquisitions in patients. It is likely that the cutoff frequency, within reasonable limits, little affected the results returned by Doppler vortography, because we were interested in the frames with relatively high velocities (E wave). A better alternative to suppress clutter signals, however, would be the use of efficient adaptive filters such as eigen-based clutter filters (Yu and Cobbold 2008; Yu and Lovstakken 2010). Furthermore, the Doppler signal-to-noise ratio was generally high in most cases during early filling. Low signal-to-noise ratio Doppler images were successfully de-aliased and denoised using the robust discrete cosine transform-based smoother (Muth et al. 2011). It should be noted that denoising does not influence vortex detection significantly because of the presence of a covariance-based filter, but it is required to obtain a consistent estimate of the core vorticity, as an angular derivative is necessary (see eqn [7]). Poor image sampling could also impede vortex detection/quantification. In all patients studied, however, the Doppler sectors contained at least 50 scan lines and enclosed the inner left ventricular cavity entirely to ensure high-quality measures. This was sometimes done at the expense of frame rate, but low frame rates do not affect the technique by itself. Of note, after some practice, the vortical regions can be spotted by an experienced eye from the color Doppler cine loops only. This actually helps to fine-tune the Doppler acquisition and to better adjust the Doppler sector. Finally, it should be pointed out that the pilot clinical study reported in this article was performed in only 19 patients. Because the echographic conditions encountered in these patients were all nearly optimal (no obesity, no cardiac complication, *etc.*), one must be aware that we likely missed clinical situations in which Doppler vortography may fail. A more exhaustive analysis performed in a large group of patients, with different echographic settings (pulse repetition frequency, signal-to-noise ratio, wall filter, Nyquist velocity, *etc.*), would help to better identify the potential artifacts of Doppler vortography.

Doppler vortography as a potential clinical tool for better assessment of diastolic function

In some hypertensive patients (see Fig. 9, second row), a retrograde (*i.e.,* counter-rotating with respect to the natural flow circulation) vortex was visible in the apex, by both Doppler vortography and VFM. In other patients (such as in Fig 9, first row, normotensive subject), a large vortex was present adjacent to the posterior mitral valve leaflet. Because a slight modification of the wall and/or inflow dynamics may significantly alter intraventricular flow, we believe that vortex flow imaging by Doppler vortography could be of help in the evaluation of diastolic function. In the presence of an apical vortex, the left ventricle may enter into a vicious cycle. Because it rotates in a direction opposite that of natural flow, the apical vortex induces excessive fluid energy dissipation and, thus, increases the workload. This may further disturb the blood flow filling patterns, which, in turn, decreases the vorticity of the main vortex. It could be expected that the vorticity of the major vortex is, to some extent, negatively related to the degree of filling impairment. At this stage of the study, this assertion remains hypothetical. A prospective study in a large group of patients is necessary to determine the potential clinical interest of Doppler vortography for the assessment of diastolic function and the prediction of adverse events.

CONCLUSIONS

Doppler vortography is able to decipher the vortical structures that form in the left ventricle during diastole. This color Doppler approach may offer new echographic insights into left ventricular function, especially for diastology.

Acknowledgments—This work was supported by operating grants from the Canadian Institutes of Health Research (CIHR, MOP-106465) and the Heart and Stroke Foundation of Québec (HSFQ). Damien Garcia holds a research scholarship award from the Fonds de Recherche en Santé du Québec (FRSQ).

REFERENCES

Arigovindan M, Suhling M, Jansen C, Hunziker P, Unser M. Full motion and flow field recovery from echo Doppler data. IEEE Trans Med Imaging 2007;26:31–45.

Belohlavek M. Vortex formation time: An emerging echocardiographic index of left ventricular filling efficiency? Eur Heart J Cardiovasc Imaging 2012;13:367–369.

Carlhall CJ, Bolger A. Passing strange: Flow in the failing ventricle. Circ Heart Failure 2010;3:326–331.

Chan KL, Veinot JP. Assessment of diastolic function. In: Chan KL, (ed). Anatomic basis of echocardiographic diagnosis. London: Springer-Verlag; 2011. p. 421–438.

Charonko JJ, Kumar R, Stewart K, Little WC, Vlachos PP. Vortices formed on the mitral valve tips aid normal left ventricular filling. Ann Biomed Eng 2013;41:1049–1061.

Chen R, Zhao BW, Wang B, Tang HL, Li P, Pan M, Xu LL. Assessment of left ventricular hemodynamics and function of patients with uremia by vortex formation using vector flow mapping. Echocardiography 2012;29:1081–1090.

Cimino S, Pedrizzetti G, Tonti G, Canali E, Petronilli V, De Luca L, Iacoboni C, Agati L. In vivo analysis of intraventricular fluid dynamics in healthy hearts. Eur J Mech B/Fluids 2012;35:40–46.

Dabiri JO, Gharib M. The role of optimal vortex formation in biological fluid transport. Proc R Soc B 2005;272:1557–1560.

Delemarre BJ, Visser CA, Bot H, Dunning AJ. Prediction of apical thrombus formation in acute myocardial infarction based on left ventricular spatial flow pattern. J Am Coll Cardiol 1990;15:355–360.

Domenichini F, Querzoli G, Cenedese A, Pedrizzetti G. Combined experimental and numerical analysis of the flow structure into the left ventricle. J Biomech 2007;40:1988–1994.

Eriksson J, Bolger AF, Ebbers T, Carlhall CJ. Four-dimensional blood flow-specific markers of LV dysfunction in dilated cardiomyopathy. Eur Heart J Cardiovasc Imaging 2012;14:417–424.

Eriksson J, Carlhall CJ, Dyverfeldt P, Engvall J, Bolger AF, Ebbers T. Semi-automatic quantification of 4-D left ventricular blood flow. J Cardiovasc Magn Reson 2010;12:9.

Faludi R, Szulik M, D'hooge J, Herijgers P, Rademakers F, Pedrizzetti G, Voigt JU. Left ventricular flow patterns in healthy subjects and patients with prosthetic mitral valves: An in vivo study using echocardiographic particle image velocimetry. J Thorac Cardiovasc Surg 2010;139:1501–1510.

Gao H, Claus P, Amzulescu MS, Stankovic I, D'hooge J, Voigt JU. How to optimize intracardiac blood flow tracking by echocardiographic particle image velocimetry? Exploring the influence of data acquisition using computer-generated data sets. Eur Heart J Cardiovasc Imaging 2012;13:490–499.

Garcia D. Robust smoothing of gridded data in one and higher dimensions with missing values. Comput Statist Data Anal 2010;54:1167–1178.

Garcia D. Fast all-in-one method for automated post-processing of PIV data. Experiments Fluids 2011;50:1247–1259.

Garcia D, del Álamo JC, Tanné D, Yotti R, Cortina C, Bertrand E, Antoranz JC, Rieu R, Garcia-Fernandez MA, Fernandez-Aviles F, Bermejo J. Two-dimensional intraventricular flow mapping by digital processing conventional color-Doppler echocardiography images. IEEE Trans Med Imaging 2010;29:1701–1713.

Gharib M, Rambod E, Kheradvar A, Sahn DJ, Dabiri JO. Optimal vortex formation as an index of cardiac health. Proc Natl Acad Sci USA 2006;103:6305–6308.

Hendabadi S, Bermejo J, Benito Y, Yotti R, Fernandez-Aviles F, del Álamo JC, Shadden SC. Topology of blood transport in the human left ventricle by novel processing of Doppler echocardiography. Ann Biomed Eng 2013 July 2 [EPub ahead of print].

Hong GR, Pedrizzetti G, Tonti G, Li P, Wei Z, Kim JK, Baweja A, Liu S, Chung N, Houle H, Narula J, Vannan MA. Characterization and quantification of vortex flow in the human left ventricle by contrast echocardiography using vector particle image velocimetry. JACC Cardiovasc Imaging 2008;1:705–717.

Hunt JCR, Wray AA, Moin P. Eddies, streams, and convergence zones in turbulent flows. In: Proceedings, 1988 Summer Program, Stanford NASA Centre for Turbulence Research. CTR-S88 1988;193–208.

Jensen JA. Field: A program for simulating ultrasound systems. Med Biol Eng Comput 1996;34:351–353.

Jensen JA, Svendsen NB. Calculation of pressure fields from arbitrarily shaped, apodized, and excited ultrasound transducers. IEEE Trans Ultrason Ferroelectr Freq Control 1992;39:262–267.

Jiamsripong P, Calleja AM, Alharthi MS, Dzsinich M, McMahon EM, Heys JJ, Milano M, Sengupta PP, Khandheria BK, Belohlavek M. Impact of acute moderate elevation in left ventricular afterload on diastolic transmitral flow efficiency: analysis by vortex formation time. J Am Soc Echocardiogr 2009;22:427–431.

Kasai C, Namekawa K, Koyano A, Omoto R. Real-time two-dimensional blood flow imaging using an autocorrelation technique. IEEE Trans Son Ultrason 1985;32:458–464.

Kheradvar A, Assadi R, Falahatpisheh A, Sengupta PP. Assessment of transmitral vortex formation in patients with diastolic dysfunction. J Am Soc Echocardiogr 2012;25:220–227.

Kheradvar A, Pedrizzetti G. Vortex formation in the cardiovascular system. London: Springer-Verlag; 2012.

Kilner PJ, Yang GZ, Wilkes AJ, Mohiaddin RH, Firmin DN, Yacoub MH. Asymmetric redirection of flow through the heart. Nature 2000;404:759–761.

Kim HB, Hertzberg JR, Shandas R. Development and validation of echo PIV. Experiments Fluids 2004;36:455–462.

Lu J, Li W, Zhong Y, Luo A, Xie S, Yin L. Intuitive visualization and quantification of intraventricular convection in acute ischemic left ventricular failure during early diastole using color Doppler-based echocardiographic vector flow mapping. Int J Cardiovasc Imaging 2012;28:1035–1047.

Markl M, Kilner PJ, Ebbers T. Comprehensive 4-D velocity mapping of the heart and great vessels by cardiovascular magnetic resonance. J Cardiovasc Magn Reson 2011;13:7.

Mitchell DG. Color Doppler imaging: Principles, limitations, and artifacts. Radiology 1990;177:1–10.

Mohiaddin RH. Flow patterns in the dilated ischemic left ventricle studied by MR imaging with velocity vector mapping. J Magn Reson Imaging 1995;5:493–498.

Muth S, Dort S, Sebag IA, Blais MJ, Garcia D. Unsupervised dealiasing and denoising of color-Doppler data. Med Image Anal 2011;15:577–588.

Nucifora G, Delgado V, Bertini M, Marsan NA, Van de Veire NR, Ng AC, Siebelink HM, Schalij MJ, Holman ER, Sengupta PP, Bax JJ. Left ventricular muscle and fluid mechanics in acute myocardial infarction. Am J Cardiol 2010;106:1404–1409.

Pedrizzetti G, Domenichini F. Nature optimizes the swirling flow in the human left ventricle. Phys Rev Lett 2005;95:108101.

Poh KK, Lee LC, Shen L, Chong E, Tan YL, Chai P, Yeo TC, Wood MJ. Left ventricular fluid dynamics in heart failure: Echocardiographic measurement and utilities of vortex formation time. Eur Heart J Cardiovasc Imaging 2012;13:385–393.

Prinz C, Faludi R, Walker A, Amzulescu M, Gao H, Uejima T, Fraser AG, Voigt JU. Can echocardiographic particle image velocimetry correctly detect motion patterns as they occur in blood inside heart chambers? A validation study using moving phantoms. Cardiovasc Ultrasound 2012;10:24.

Raffel M, Willert C, Wereley S, Kompenhans J. Post-processing of PIV data. In: Particle image velocimetry, (ed). A practical guide. Berlin/New York: Springer-Verlag; 2007. p. 177–208.

Rodevand O, Bjornerheim R, Edvardsen T, Smiseth OA, Ihlen H. Diastolic flow pattern in the normal left ventricle. J Am Soc Echocardiogr 1999;12:500–507.

Sengupta PP, Pedrizzetti G, Kilner PJ, Kheradvar A, Ebbers T, Tonti G, Fraser AG, Narula J. Emerging trends in CV flow visualization. JACC Cardiovasc Imaging 2012;5:305–316.

Stewart KC, Charonko JC, Niebel CL, Little WC, Vlachos PP. Left ventricle filling vortex formation is unaffected by diastolic impairment. Am J Physiol Heart Circ Physiol 2012;303:H1255–H1262.

Tanné D, Bertrand E, Kadem L, Pibarot P, Rieu R. Assessment of left heart and pulmonary circulation flow dynamics by a new pulsed mock circulatory system. Experiments Fluids 2010;48:837–850.

Thompson RB, McVeigh ER. Fast measurement of intracardiac pressure differences with 2-D breath-hold phase-contrast MRI. Magn Reson Med 2003;49:1056–1066.

Töger J, Kanski M, Carlsson M, Kovács SJ, Söderlind G, Arheden H, Heiberg E. Vortex ring formation in the left ventricle of the heart: Analysis by 4-D flow MRI and Lagrangian coherent structures. Ann Biomed Eng 2012;40:2652–2662.

Uejima T, Koike A, Sawada H, Aizawa T, Ohtsuki S, Tanaka M, Furukawa T, Fraser AG. A new echocardiographic method for identifying vortex flow in the left ventricle: numerical validation. Ultrasound Med Biol 2010;36:772–788.

Van Dantzig JM, Delemarre BJ, Bot H, Koster RW, Visser CA. Doppler left ventricular flow pattern versus conventional predictors of left ventricular thrombus after acute myocardial infarction. J Am Coll Cardiol 1995;25:1341–1346.

Wigstrom L, Ebbers T, Fyrenius A, Karlsson M, Engvall J, Wranne B, Bolger AF. Particle trace visualization of intracardiac flow using time-resolved 3-D phase contrast MRI. Magn Reson Med 1999; 41:793–799.

Yu A, Lovstakken L. Eigen-based clutter filter design for ultrasound color flow imaging: A review. IEEE Trans Ultrason Ferroelectr Freq Control 2010;57:1096–1111.

Yu AC, Cobbold RS. Single-ensemble-based eigen-processing methods for color flow imaging: Part I. The Hankel-SVD filter. IEEE Trans Ultrason Ferroelectr Freq Control 2008;55: 559–572.

Zhang H, Zhang J, Zhu X, Chen L, Liu L, Duan Y, Yu M, Zhou X, Zhu T, Zhu M, Li H. The left ventricular intracavitary vortex during the isovolumic contraction period as detected by vector flow mapping. Echocardiography 2012;29:579–587.